Available online at www.sciencedirect.com
ScienceDirect
Scripta Materialia 64 (2011) 502–505
Scripta MATERIALIA
www.elsevier.com/locate/scriptamat

Dynamic strain aging in a new Ni–Co base superalloy

C.Y. Cui,* Y.F. Gu, Y. Yuan and H. Harada

High Temperature Materials Center, National Institute for Materials Science, Sengen 1-2-1, Tsukuba 305-0047, Japan

Received 8 October 2010; revised 12 November 2010; accepted 12 November 2010
Available online 17 November 2010

Dynamic strain aging (DSA) in a newly developed Ni–Co superalloy, TMW-2, was examined at temperatures ranging from room temperature to 600 °C and strain rates between 3×10^{-2} and 8×10^{-5} s^{-1}. The alloy exhibited both normal and inverse DSA effects at the temperatures and strain rates tested. Transmission electron microscopy evidence suggests that the normal behavior is associated with conventional DSA due to dynamic dislocation–solute interaction, while the inverse behavior may be related to the occurrence of stacking faults.

Keywords: Forming processes-forging; Tension test; Nickel alloys; Dynamic strain aging

Serrated flow or the Portevin–Le Chatelier (PLC) effect during plastic deformation has been observed in various kinds of metals and alloys, from binary systems [1,2] to more complicated commercial alloys [3,4]. The dynamic interaction between mobile dislocations and diffusing solute atoms was commonly accepted to be responsible for so-called dynamic strain aging (DSA). McCormick [5] considered the jerky nature of the thermally activated motion of dislocations, and assumed that solute–dislocation interaction occurred at obstacles where dislocations were piled up.

Recently, new Ni–Co superalloys, termed TMW alloys, have been successfully developed for aircraft engines and industrial gas turbine applications. The heat resistance of TMW alloys, 725 °C, is the highest reported to date, exceeding that of the existing high-strength C&W Ni-base alloy U720Li by 50 °C [6–8]. Unlike blades, which are relatively smaller components that are wholly exposed to a narrow range of high temperatures, turbine disks are large components in the turbine and experience a spectrum of temperatures, ranging from lower temperatures at the bore, intermediate temperatures in the web to higher temperatures at the rim. It was therefore very important to study the mechanical properties of the alloy TMW-2 at these three temperature ranges. While the creep behavior of TMW alloy at elevated temperatures has been studied [9], the mechanical properties at low and intermediate temperatures had yet to be investigated.

The TMW-2 superalloys contain substitutional (Cr, Mo, Co, Al, Ti and W) and interstitial elements (C and B) and provide an opportunity to study the characteristics of DSA in the combined presence of these elements. Further, TMW-2 has a low stacking fault (SF) energy, due to the addition of high amounts of Co (>20 wt.%) [10], and thus the effect of SFs on the deformation characteristics of DSA was also examined. Because TMW alloy was intended for critical turbine disk application, it was very important to understand the extent to which DSA affects its tensile properties. Thus, the purpose of this study was to report the tensile properties and observation of DSA effect, especially the inverse DSA effect, in the superalloy TMW-2.

The nominal composition of the superalloy TMW-2 is listed in Table 1. The processing of TMW alloy was reported in Ref. [7]. The forged ingot was heat-treated at 1100 °C for 4 h (air cooling), followed by aging at 650 °C for 24 h (air cooling) and 760 °C for 16 h (air cooling). The grain size of the superalloy TMW-2 was about 10 μm, and the alloy consisted of primary γ′ precipitates (volume fraction: 16.6%; size: 0.5–2 μm) at the grain boundaries of the γ matrix, intragranular secondary γ′ precipitates (about 100 nm) and fine tertiary precipitates (about 15 nm) [7].

All tensile tests were performed on specimens with a gage section of 3 (diam.) × 16 mm. Tensile tests were performed on a Shimadzu 250KN machine at room temperature (RT), 300, 350, 400, 450, 500, 550 and

* Corresponding author. Present address: Superalloys Division, Institute of Metal Research, Shenyang 110016, People's Republic of China. Tel.: +81 29 859 2544; fax: +86 24 8397 8292; e-mail: chycui@imr.ac.cn

1359-6462/$ - see front matter
doi:10.1016/j.scriptamat.2010.11.025

Table 1. Nominal chemical composition of the superalloy TMW-2.

Alloy	Ni	Co	Cr	Mo	W	Ti	Al	C	B	Zr
TMW-2	Bal.	21.8	14.4	2.7	1.1	6.2	2.3	0.02	0.02	0.03

600 °C, and with initial strain rates ranging from 3×10^{-2} to $8 \times 10^{-5} s^{-1}$, respectively. All tensile tests were started after holding the specimen for 30 min at the test temperature. Samples for optical microscopy were prepared using conventional metallographic procedures and chemically etched by Kalling solution. Fracture surfaces were observed by scanning electron microscopy in a Philips microscope. Transmission electron microscopy (TEM) disks about 300 μm thick were cut from the samples perpendicular to the tensile axis. The disks were then manually ground down to 50 μm and perforated with a twin-jet electropolisher at 40 V and 0 °C. The electrolyte consisted of 50 ml perchloric acid, 100 ml ethanol and 300 ml 2-butoxyethanol. TEM observations were carried out on a Tecnai 20 TEM operated at 200 kV.

Figure 1a shows the typical true stress–true strain curves obtained at various temperatures at a strain rate of $3 \times 10^{-4} s^{-1}$. Serrated stress–strain curves were observed at test temperatures ranging from 300 to 500 °C, typified by the curve for 400 °C. The stress–strain curve at temperature outside of this range was smooth. Figure 1b shows the typical type A, B, and C serrations [11] observed in the stress–strain curve. Type C serrations were observed predominantly in the superalloy TMW-2 for most of the temperatures and strain rates studied, i.e. $T \geqslant 400$ °C and $\dot{\varepsilon} \leqslant 3 \times 10^{-3} s^{-1}$. Type A serrations were observed at $T = 350$ °C. At 400, 450 and 500 °C, type B serrations of very small magnitude could also be observed, though these disappeared at higher strains.

Serrated flow is generally seen to occur after a critical true plastic strain, ε_c, is reached. The strain corresponding to the peak of the first serrations was taken as the critical true plastic strain, ε_c, for onset of serrations. ε_c ranged mainly between 0.4% and 5%, depending on temperature and strain rate. Figure 2 shows the variation of ε_c with $\dot{\varepsilon}$ at various temperatures within the DSA regime. Two trends are visible in Figure 2: one associated with increasing ε_c with increasing $\dot{\varepsilon}$ and decreasing T, which was termed normal DSA; and another associated with increasing ε_c with decreasing $\dot{\varepsilon}$ and increasing T, which was termed the inverse DSA effect [12]. The normal DSA effect was observed at high $\dot{\varepsilon}$ and/or low T, while the inverse DSA effect was observed at high T and low $\dot{\varepsilon}$. It should be mentioned that the serrations observed at ε_c were of type A in the normal DSA regime, whereas they were of type C in the inverse DSA regime.

Figure 3a shows the variation of yield stress and ultimate tensile strength (UTS) of the superalloy TMW-2 at a strain rate of $3 \times 10^{-4} s^{-1}$ for test temperatures ranging from RT to 750 °C. The yield stress was slightly affected throughout this temperature range, while the UTS began decreasing gradually from 500 °C, and decreased markedly at temperatures above 600 °C. The effect of strain rate on the mechanical properties was also examined at 400 and 450 °C; the results showed that the variation in yield stress and UTS followed a trend similar to that at a strain rate of $3 \times 10^{-4} s^{-1}$ (Fig. 3a), which signified the prevalence of negative strain rate sensitivity (SRS). Based on this observation, the SRS, m, was examined using stress–strain data from tensile tests at a constant cross-head speed, as shown in Figure 3b. While m values were positive at RT and 600 °C where the stress–strain curves were smooth, m values were negative at all temperatures at which DSA occurred.

Fractographic observations and stress–strain curves (Fig. 1) showed that no necking happened before fracture in the DSA regime. Fracture surfaces of specimens showed the presence of equiaxed dimples in both the normal DSA and inverse DSA regimes. These observations suggest that characteristics of fracture in the inverse DSA regime did not differ from those in the normal DSA regime.

Detailed microstructural investigations were carried out to understand the different deformation mechanisms operating in normal and inverse DSA. In the normal DSA regime, a high density of dislocations was formed in the γ matrix and it was difficult to shear the secondary γ′ precipitate, as shown in Figure 4a. In contrast, SFs

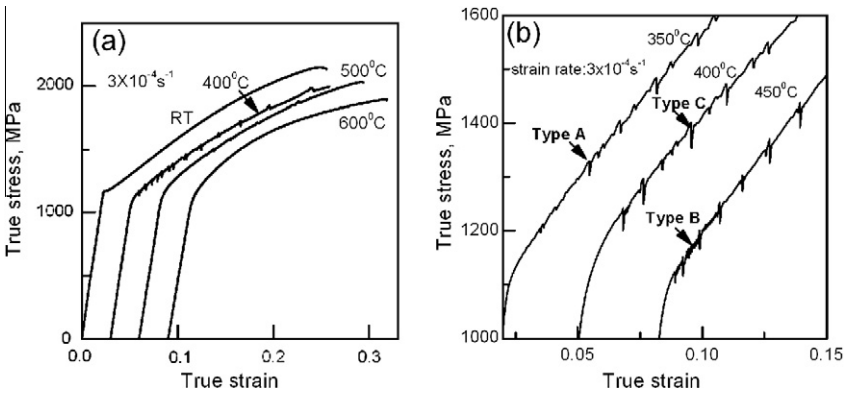

Figure 1. (a) Typical true stress–true strain curves at a strain rate of $3 \times 10^{-4} s^{-1}$. (b) Enlarged true stress–true strain curves, showing the types of serration.

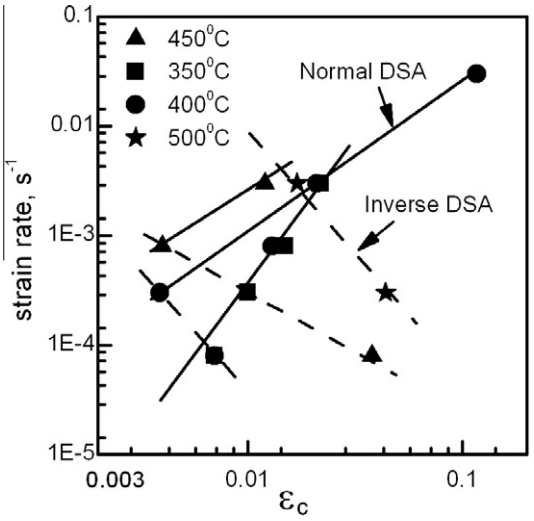

Figure 2. Variation of critical strain, ε_c for onset of serration with strain rate and temperature. The straight lines show normal DSA, and the dashed lines show inverse DSA.

were present in the inverse DSA regime, and γ′ precipitates were sheared by nearly continuous SFs, as shown in Figure 4b.

Serrated flow, precipitate shearing (Fig. 4b) and negative SRS may be related to the "pseudo-PLC effect" [13,14]. The deformation-induced dissolution of strengthening precipitates was suggested to be responsible for the pseudo-PLC effect, which has been observed in an Al–Li alloy strengthened by fine precipitates. According to the diffusion-controlled growth and shrinkage of precipitate in the Al–Li alloy, the pseudo-PLC effect possibly occurred at the low temperature at which tensile tests are performed. However, it is impossible that the stable γ′ precipitate in TMW-2 would dissolve or reprecipitate at temperatures lower than 500 °C. In addition, the negative strain rate dependence was reported in Al–Mg alloy as one of the manifestations of the conventional DSA effect [15]. Hence, we suppose that the serrated flow in the superalloy TMW-2 is a result of DSA.

Up to now, ε_c with T and $\dot{\varepsilon}$ in the normal DSA regime has been modeled [16], and inverse behavior has not yet been well understood. Normal and inverse DSA effects were also found in other Ni-base superalloys, such as Waspaloy [2,4] and U720Li [17]. Hayes and Hayes proposed [2,4] that the change from normal to inverse behavior was a result of interactions between carbon atmospheres and the strengthening precipitates, i.e. γ′-Ni_3Al in Waspalloy. In this case, the precipitates act

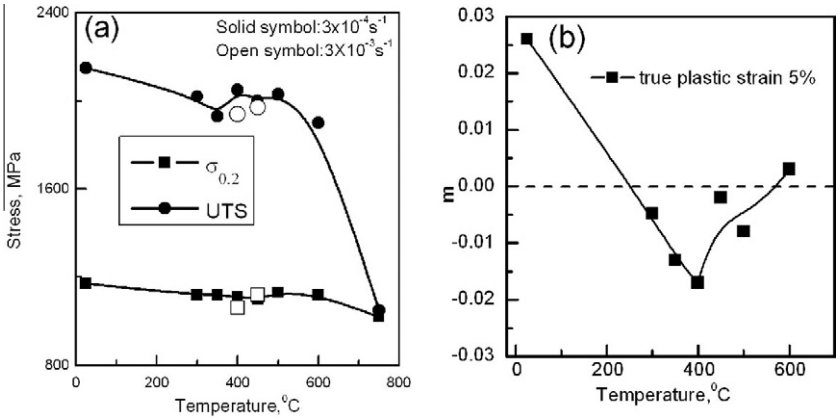

Figure 3. (a) Variation of yield stress and ultimate tensile strength with temperature. (b) The strain rate sensitivity, m, was plotted as a function of temperature at a true plastic strain of 5%.

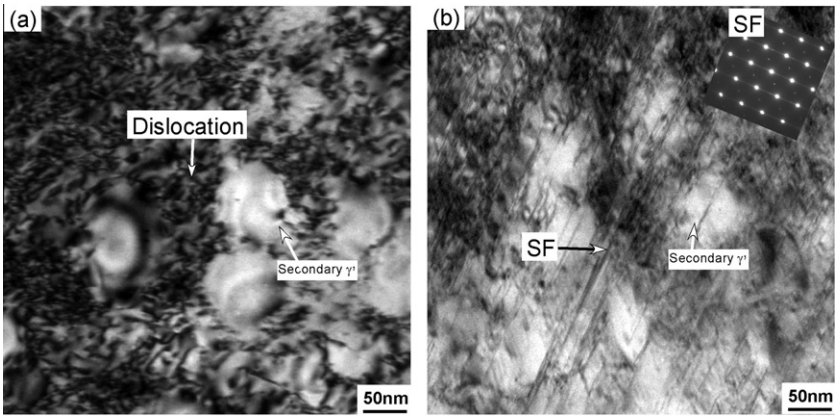

Figure 4. TEM observations on the deformed samples tested at 450 °C and a strain rates of (a) 3×10^{-3} s^{-1}, showing the high density of dislocations occurring in the normal DSA regime, and (b) 8×10^{-5} s^{-1}, showing that the γ′ precipitates were sheared by the continuous SFs.

as a sink for carbon, which diffuses down the dislocation line to the sink, while the line is arrested at the precipitates. Gopinath et al. [17], however, ascribed the locking of the mobile dislocations by substitutional alloy elements to be responsible for the DSA. Hale et al. [18], from an estimation of the activation energy, identified that the lattice diffusion of interstitial C atoms at lower temperatures (173–473 °C) and of substitutional Cr atoms at higher temperatures (523–673 °C) is responsible for serrated flow in Inconel 718 alloy. From the brief literature survey, a consensus exists as to the mechanism (diffusion of the interstitial C atoms) responsible for serrated flow at low temperatures, while for higher temperatures there is divergence of opinion as to which element is responsible for DSA.

So far, the effects of planar defects, such as SFs, on DSA have rarely reported in the literature. In the present study, a high density of SFs was found not in the normal DSA regime, but in the inverse DSA (Fig. 4b), probably due to the low SF energy in TMW-2. Thus, there was probably a correlation between the high density of SFs with the inverse DSA effect in the Ni–Co-base superalloy TMW-2. Further work is needed to clarify the effect of SF motion on DSA, particularly on inverse DSA.

In summary, the superalloy TMW-2 exhibited serrated flow during tensile deformation due to DSA within an intermediate temperature range of 350–500 °C. In the serrated flow regime, the alloy clearly exhibits negative SRS, and both normal and inverse DSA occur. Tensile properties in the DSA regime, such as yield stress, UTS and fracture features, are not influenced by temperature and strain rate. A correlation between a high density of SFs and the inverse DSA effect is found in superalloy TMW-2 which has a low SF density.

This work was partly supported by "Hundreds of Talents Project" and the National Basic Research Program (973 Program) of China under Grant No. 2010CB631200 (2010CB631206).

[1] T. Tabata, H. Fujita, Y. Nakajima, Acta Metall. 28 (1980) 795.
[2] R.W. Hayes, W.C. Hayes, Acta Metall. 30 (1982) 1295.
[3] E. Bouchaud, L. Kubin, H. Octor, Metall. Trans. 22A (1991) 1021.
[4] R.W. Hayes, Acta Metall. 31 (1983) 365.
[5] P.G. McCormick, Acta Metall. 20 (1972) 351.
[6] C.Y. Cui, Y.F. Gu, H. Harada, A. Sato, Metall. Mater. Trans. A 36A (2005) 2921.
[7] Y.F. Gu, T. Fukuda, C. Cui, H. Harada, A. Mitsuhashi, T. Yokokawwa, J. Fujioka, Y. Koizumi, T. Kobayashi, Metall. Mater. Trans. A 40A (2009) 3047.
[8] C.Y. Cui, Y.F. Gu, D.H. Ping, H. Harada, Metall. Mater. Trans. A 40A (2009) 282.
[9] Y.F. Gu, C. Cui, D. Ping, H. Harada, T. Fukuda, J. Fujioka, Mater. Sci. Eng. A A510–511 (2009) 250.
[10] Y. Yuan, Y.F. Gu, C.Y. Cui, T. Osada, T. Tetsui, T. Yokokawa, H. Harada, Adv. Engg. Mater. in press.
[11] P. Rodriguez, Bull. Mater. Sci. 6 (1984) 653.
[12] Y. Brechet, Y. Estrin, Acta Metall. Mater. 43 (1995) 955.
[13] Y. Brechet, Y. Estrin, Scripta Metall. Mater. 31 (1994) 185.
[14] Y. Brechet, Y. Estrin, Scripta Metall. Mater. 35 (1996) 217.
[15] P.G. McCormick, Scripta Metall. 4 (1970) 221.
[16] J.M. Robinson, M.P. Shaw, Inter. Mater. Rev. 39 (1994) 113.
[17] K. Gopinath, A.K. Gogia, S.V. Kamat, U. Ramamurty, Acta Mater. 57 (2009) 1243.
[18] C.L. Hale, W.S. Rollings, M.L. Weaver, Mater. Sci. Eng. A 300A (2001) 153.